RSC Advances

ROYAL SOCIETY OF CHEMISTRY

www.rsc.org/advances

Journal Name

RSCPublishing

ARTICLE

Sprayable, Paintable Layer-by-Layer Polyaniline Nanofiber/Graphene Electrodes

Cite this: DOI: 10.1039/x0xx00000x

Se Ra Kwon,[†] Ju-Won Jeon,[†] and Jodie L. Lutkenhaus[*]

Received 00th January 2012,
Accepted 00th January 2012

DOI: 10.1039/x0xx00000x

www.rsc.org/

Using polyaniline nanofibers and graphene oxide sheets, we demonstrate here the successful layer-by-layer (LbL) assembly of the two anisotropic nanomaterials using a water-based spray-on approach. The processing parameters most critical to the production of uniform electrodes are blow-drying time and removal of the rinsing step. The resulting polyaniline nanofiber/graphene oxide films are electrochemically reduced to convert graphene oxide to reduced graphene oxide, as evidenced by a distinctive change in colour and Raman spectra. The architecture of the electrode is highly porous (72% void), which facilitates ion transport. The electrodes' ability to store charge is evaluated as a function of thickness in non-aqueous conditions ($LiClO_4$ in propylene carbonate, lithium metal anode). The capacity reaches values as high as 114 mAh/g (45 mAh/cm^3) at 0.03 A/g. Besides capacity, other performance metrics (energy and power) are compared against control electrodes made by a different processing approach, dip-assisted LbL assembly. It is found that spray-assisted LbL assembly is over 70 times faster and yields electrodes with better rate capability relative to dip-assisted LbL assembly.

INTRODUCTION

Structural energy and power, in which a battery or capacitor is seamlessly integrated into the object it powers, is receiving more and more attention. The general concept is to design a battery and its form factor around the device rather than *vice versa*. Spray-on approaches are particularly interesting in this regard because they offer large-area coverage onto complex surfaces.[1-4] It is desirable to use water as the spraying medium, as it limits the use of alternative volatile or costly solvents. To this end, it is critical to identify a water-based spray-on process that is suitable for anisotropic nanomaterials such as polyaniline nanofibers (PANI NFs) and functionalized graphene sheets, which are often investigated as electrode materials.

Polyaniline (PANI) is a p-type conjugated polymer, and has long been explored as a cathodic material for lithium metal and lithium-ion batteries and as a pseudocapacitive material for supercapacitors. PANI is an intrinsic conductor and is redox-active, storing charge through a reversible doping-dedoping mechanism.[5-7] PANI NFs, which tend to generate porous architectures, have been investigated as electrodes for electrochemical energy storage.[7-13] Examples of such electrodes include PANI NF/V_2O_5,[5] PANI NF/multiwall carbon nanotubes (MWNTs),[14] and PANI NF/graphene[7, 15, 16] This study focuses specifically upon water-processable PANI NFs, which are 30-50 nm in diameter and 100-500 nm long.[17] Their small size and stability in water renders them excellent candidates for spray-on processing.

Graphene is a two-dimensional carbon sheet, and has been considered a promising material due to its high electrical and thermal conductivities, mechanical strength, and specific surface area.[18-20] Graphene and graphene-based composite materials have been proposed for use in energy storage and generation devices such as batteries, supercapacitors, fuel cells, and solar cells.[21-23] It has been shown that the composite materials containing nanostructured graphene and conducting polymers can significantly improve the electrochemical performance due to their nanoarchitecture which provides increased surface area for charge storage ad less diffusion limitation for ionic and electronic transport.[24, 25] However, pristine graphene sheets are challenging to suspend and process, especially in water. Instead, it is more practical to utilize graphene oxide (GO) sheets, which bear oxygen-containing functional groups in their basal plane and edges. GO sheets can be reduced chemically, thermally, or electrochemically to yield reduced graphene oxide (RGO).[16, 26-28] Energy storage in RGO electrodes proceeds by both capacitive (electrical double layer) and pseudocapacitive (*via* remnant oxygen-containing functional groups) mechanisms.[21, 23, 29-31]

Thus, there have been great efforts to fabricate hybrid electrodes containing both PANI NFs and graphene *via* various methods such as *in-situ* chemical polymerization of aniline with graphene,[15, 32, 33] vacuum filtration,[7, 34, 35] and layer-by-layer (LbL) assembly.[16] With the exception of LbL assembly, none of

these techniques have proven suitable for large-area deposition *via* spraying or comparable methods.

LbL assembly is a powerful and versatile tool for the fabrication of multi-component hybrid electrodes. In LbL assembly, the film or electrode is fabricated *via* alternate exposure of a substrate to oppositely charged (or complementary) species from solutions or dispersions. Film properties such as thickness, composition, and structure can be precisely controlled by deposition conditions.[36] The LbL process has been utilized in the deposition of electrodes for batteries and supercapacitors. The motivation is that LbL assembly allows for molecular-level mixing of the adsorbing species, leading to synergistic effects between the two.[16, 27, 33, 37] Examples include PANI/MWNT,[14] MWNT/graphene,[38] MWNT/MnO_2,[39] and MWNT/MWNT[3, 40] electrodes, for which dip-assisted LbL assembly was employed for all. Dip-assisted LbL assembly relies upon immersion of the substrate, as compared to spraying of the substrate as is done for spray-assisted LbL assembly. The former approach has encountered challenges with slow processing, cross-contamination of baths, and cumbersome handling of large-scale substrates.[41] The latter process is faster, eliminates cross-contamination, and can be scaled up to large-area substrates.[3, 4, 41-43] Spray-assisted LbL assembly has been proposed for applications such as drug delivery,[44] anti-reflection coatings,[45] and light-emitting diodes.[46]

Recently, we reported on the fabrication of PANI NF/electrochemically reduced graphene oxide (ERGO) electrodes made via dip-assisted LbL assembly.[16] These electrodes performed quite well as cathodes in lithium metal batteries, but the dipping process remains cumbersome. For the purposes of large-scale deposition and potential integration into flexible or complex substrates, we were motivated to assemble analogous electrodes via spray-assisted LbL assembly and compare their performance to their predecessor. To date, there exists only two reports on electrodes fabricated from spray-assisted LbL assembly including PANI NF/V_2O_5 and $MWNT^+/MWNT^-$ electrodes.[4, 32] To our knowledge, there are very few reports[47-49] on spray-assisted LbL assembly with GO sheets, perhaps because they are somewhat difficult to assemble into a uniform film.

Herein, we present PANI NF/ERGO electrodes fabricated via spray-assisted LbL assembly for the first time. These electrodes are formed by the alternate spraying of positively charged PANI NFs and negatively charged GO sheets. Best practices towards the spraying and assembly of these components is first presented, in which film growth is characterized by profilometry, quartz crystal microbalance (QCM), scanning electron microscopy (SEM), and Raman spectroscopy. Following assembly, the GO sheets are electrochemically reduced to ERGO to produce a PANI NF/ERGO electrode. The results of the electrochemical reduction step are presented, followed by the charge storage behaviour of these electrodes in a nonaqueous half-cell with lithium as the anode (i.e., lithium metal battery). Results are compared to analogous electrodes made previously by dip-assisted LbL assembly.

EXPERIMENTAL SECTION

Materials

Aniline, ammonium peroxydisulfate, propylene carbonate, lithium perchlorate, potassium permanganate, sodium nitrate, and hydrazine were purchased from Sigma Aldrich. Li foil was purchased from Alfa Aesar. Linear polyethyleneimine (PEI, Mw ~25,000) and poly(acrylic acid) (PAA, Mw ~50,000, 25% aqueous solution) were purchased from Polysciences. Graphite (SP-1) was purchased from Bay Carbon. Indium-tin oxide (ITO)-coated glass (resistance <20 Ω/sq) and In_2O_3/Au/Ag-coated PET film (resistance <10 Ω/sq) were purchased from Delta Technologies. Microporous poly(propylene) separator (Celgard 3501) was provided by Celgard.

Preparation of PANI NF and GO dispersions

PANI NFs were synthesized using a rapid mixing approach.[17] Aniline (1.49 g, 16 mmol) was dissolved in 50 mL of 1 M HCl solution. Ammonium peroxydisulfate (0.915 g, 4 mmol) was dissolved in 50 mL of 1 M HCl solution. Both solutions were purged with nitrogen for 1 h at room temperature. Then, ammonium peroxydisulfate solution was rapidly mixed with aniline solution under nitrogen, and the mixed solution was stirred for 24 h at room temperature. After polymerization, the resulting deep-green PANI NF dispersion was dialyzed against deionized water for three days. For LbL assembly, the PANI NF dispersion was diluted to 0.5 mg/mL with deionized water, and the pH value was adjusted to 2.5.

Graphite oxide was synthesized using a modified Hummers method.[50] 3 g of graphite powder was put into cold, concentrated 120 mL of H_2SO_4. 2.5 g of $NaNO_3$ was added and stirred for 5 h in an ice water bath. Then, 15 g of $KMnO_4$ was gradually added to the mixture under stirring and cooling with ice so that the temperature of the mixture was kept below 20 ^oC. Then, the mixture was stirred at 35 ^oC for 2 h and diluted with 250 mL of cold deionized water. 700 mL of deionized water and 20 mL of 30 wt% H_2O_2 was added to the mixture, and the reaction mixture became brown in color. The mixture was washed with 5 wt% HCl solution and filtered. The filtered mixture was re-dispersed in deionized water and dialyzed. Graphite oxide power was obtained after the resulting dispersion was dried at 60 ^oC. The graphite oxide powder was dissolved in deionized water (0.5 mg/mL) and exfoliated via sonication to give GO sheets in dispersion.

Preparation of PANI NF/GO spray-assisted LbL films

PANI NF/GO spray-assisted LbL films were fabricated on ITO-coated glass using an automated spray-assisted LbL system (Svaya Nanotechnologies). ITO-coated glass substrates were cleaned *via* sequential sonication in dichloromethane, acetone, methanol, and deionized water for 15 min each. Then, the substrates were dried in a convection oven, followed by 5 min of oxygen plasma treatment (Harrick PDC-32G). For LbL assembly, two layer pairs of PEI and PAA were sprayed onto the clean substrates as base-layers. 20 mM of PEI in water (pH

4) was sprayed for 10 s, followed by rinsing with water (pH 4) for 10 s. The same processes were then carried out with 20 mM of PAA in water (pH 4) and rinsing as before. After the base-layers were deposited, PANI NF/GO spray-assisted LbL films were fabricated. The PANI NF dispersion (0.5 mg/mL, pH 2.5) was sprayed onto the substrate for 10 s, followed by blow-drying with air, then the GO dispersion (0.5 mg/mL, pH 3.5) was sprayed for 10 s, followed by blow-drying. The above procedure was repeated to achieve the desired number of layer pairs. The dispersions and blown air were applied with regulated pressure of 25 psi. Electrochemical reduction was carried out by holding the LbL film at 1.5 V vs. Li/Li^+ in a three-electrode cell as described below.

Materials characterization

Thickness was measured using a profilometer (P-6, KLA-Tencor) from at least 10 selected points per sample and averaged. The mass density of the LbL film was measured using a quartz crystal microbalance (Maxtek-RQCM, Inficon). Raman spectra were recorded using a Raman spectrometer (Horiba Jobin Yvon). Morphologies of the LbL films were investigated using a field-emission scanning electron microscope (FESEM) (JSM-7500F, JEOL).

Electrochemical characterization

After the LbL films were fabricated, they were dried in air for 24 h and then under vacuum before electrochemical testing. Electrochemical properties were measured using either three-electrode cells or two-electrode sandwich cells. For the three-electrode cell, the spray-assisted LbL electrode on ITO-coated glass was used as the working electrode and two Li foils were used as counter and reference electrodes. As an electrolyte, 0.5 M $LiClO_4$ in propylene carbonate (PC) was used. The two-electrode sandwich cell was comprised of the spray-assisted LbL electrode on ITO-coated glass as a cathode, Li foil anode, a poly(propylene) separator, and 1 M $LiClO_4$ in PC as the electrolyte. All electrochemical tests were performed using a potentiostat (SI 1287, Solatron) at room temperature in an argon-filled, oxygen- and water-free argon-filled glove box (MBraun). The average active area was 2.45 cm^2, and typical electrode masses were 1.2 $\mu g/cm^2$ with variations depending on the number of layers deposited.

RESULTS AND DISCUSSION

Spray-Assisted LbL Assembly of PANI NFs and GO Sheets

Positively charged PANI NFs and negatively charged GO sheets were alternately sprayed from water-based dispersions onto ITO-coated glass slides. In spray-assisted LbL assembly, film deposition can be affected by several parameters including concentration, spraying time, rinsing time, and air-blowing time.[4, 43, 51] For this present system, we found that rinsing and blow-drying times affect the quality of the film most significantly. Any amount of rinsing caused the films to delaminate and deconstruct. Figure S1a shows an example, where the film had deconstructed during growth, leaving behind patches of film. Accordingly, the rinsing step was eliminated in favour of blow-drying. An intermediate blow-drying time of 1 min was found to yield the most uniform films with steady LbL growth. Without blow-drying or rinsing, poor film growth was observed, Figure S1b. Blow-drying for 2 min resulted in uneven film growth, Figure S1c-d.

The sensitivity of LbL film quality to rinsing and blow-drying times points to the importance of balancing processing vs. adsorption timescales. Anisotropic materials require enough time to rotate, translate, and diffuse to the surface so as to adsorb at some favoured orientation. During the spraying process the substrate's surface develops a wetted film, through which the adsorbing species must diffuse. Rinsing disturbs and renews the wetted film, removing non-adsorbed anisotropic nanoparticles. If the time scale of spraying and rinsing is shorter than the time scale of the diffusion-adsorption process, then nanoparticle adsorption will be weak and poor films will result. On the other hand, blow-drying decreases the thickness of the wetted film, reducing the diffusion path and the timescale of adsorption.[4, 43]

Good-quality PANI NF/GO LbL films were constructed using the optimized spraying parameters (10 sec spraying and 1 min blow-drying for each layer), Figure 1a and Movie S1. The films were green in colour and became darker with increasing number of layer pairs, indicative of an increase in thickness as assembly continued. The film thickness was measured using profilometry for various numbers of layer pairs, in which linear growth behaviour was observed, Figure 1b. The average thickness per layer pair was 46 nm, which is comparable with the diameter of PANI NFs.[43] This value is suggestive of a single layer of PANI NFs laying parallel to the substrate, with GO sheets in between the PANI NF layers. Also, this layer pair thickness was much larger than that for films fabricated by dip-assisted LbL assembly (9 nm),[16] which were proposed to exhibit patchy adsorption and well-mixed layers. The significant difference for spraying here is that the diffusion path is shorter than that of dipping, which possibly leads to enhanced adsorption of nanoparticles and greater layer pair thickness in sprayed films. This result leads to 74-fold enhancement of the growth rate for spray vs. dip-assisted LbL assembly (0.29 nm/s vs. 0.0039 nm/s, respectively).

The incremental mass adsorbed per layer was measured after each adsorption step using quartz crystal microbalance (QCM), allowing for an estimation of the composition. Similar to the trend in the thickness, the mass of the LbL film increased linearly (1.25 $\mu g/cm^2$ per layer pair) as assembly continued, the mass of 100-layer pair film was 124.84 $\mu g/cm^2$. The composition of the film was approximately 67 wt% PANI NF and 33 wt% GO sheets, Figure 1c. From the area, thickness per layer pair, and mass per layer pair, the average density of the spray-assisted LbL films was calculated to be 0.4 g/cm^3, suggestive of a porous architecture. This value is lower than that of analogous films made by dipping (0.56 g/cm^3).[16] The void fraction of the spray-assisted LbL electrode was estimated

to be 0.74 from the density of the composite electrode, polyaniline (1.329 g/cm^3), and GO sheets (2.2 g/cm^3).[23]

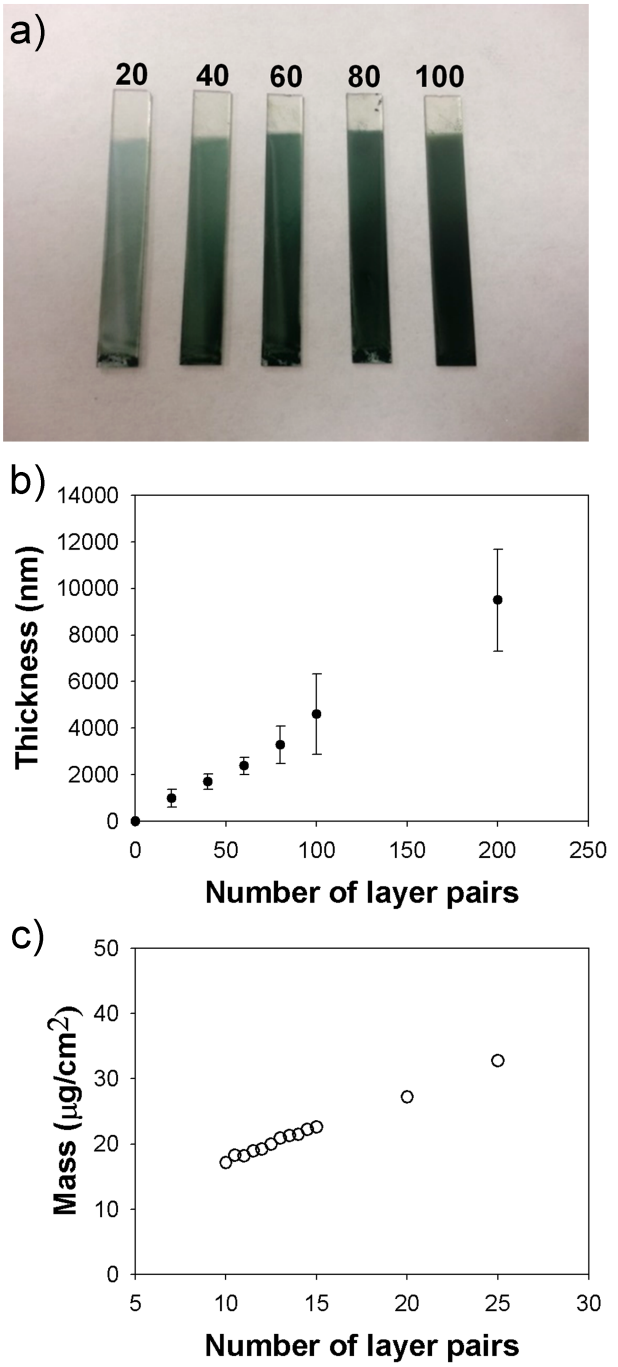

Figure 1. (a) Digital image of the PANI NF/GO spray-assisted LbL films with varying number of layer pairs. (b) Thickness and (c) mass of spray-assisted PANI NF/GO LbL films as measured using profilometry and QCM, respectively.

The morphology of the PANI NF/GO spray-assisted LbL film was investigated using SEM. Figure 2a shows a top-view SEM image of the PANI NF/GO spray-assisted LbL film, in which GO sheets comprised the outermost layer. The opaque regions are consistent with GO sheets, and the surface morphology of the film was rough probably due to the PANI NFs just below the GO sheets. In addition, a cross-sectional SEM image of the film confirmed the presence of both PANI NFs and GO, where the PANI NFs were sandwiched between GO sheets, Figure 2b.

To demonstrate the versatility of the process, the spray-assisted LbL technique was applied to a flexible conductive PET substrate, Figure 2c. The film did not display any obvious cracks or delamination during flexure. On the contrary, conventional dip-assisted LbL on the same substrate using PANI NFs and chemically RGO sheets was unsuccessful because of severe film delamination and aggregation. Thus, the spray-assisted LbL process can address specific challenges found in dipping and can broaden the versatility and processability for the substrates and the depositing materials.

Electrochemical Reduction and Energy Storage Performance

As-prepared PANI NF/GO spray-assisted LbL films were electrochemically reduced at 1.5 V *vs*. Li/Li$^+$ in 0.5 M $LiClO_4$ in propylene carbonate for 10 h.[16] After electrochemical reduction, the colour of the films changed from green to black, indicating that GO was reduced to ERGO, Figure 3a.[52] Electrochemical reduction was further confirmed using Raman spectroscopy. Figure 3b shows Raman spectra of PANI NF/GO spray-assisted LbL films before and after the electrochemical reduction, together with those from PANI NFs and GO sheets. PANI NFs show characteristic peaks at 1580 cm^{-1}, 1486 cm^{-1}, 1386 cm^{-1}, and 1166 cm^{-1}, which are assigned to C=C, C=N, and C-N$^{\bullet+}$ stretching, and C-H in-plane bending, respectively.[14, 53] In GO's spectrum, the two main peaks observed were at 1335 cm^{-1} and 1590 cm^{-1}, corresponding to *D* and *G* bands, respectively. The *D* band is related to structural defects and disorder of carbon domains and the *G* band is assigned to sp^2-hybridized carbon structures.[16, 53] The presence of peaks from both PANI NFs and GO sheets in the spectra of the PANI NF/GO film confirms that both materials are incorporated into the film. The *D*/*G* intensity ratio increased for PANI NF/GO films upon electrochemical reduction from 0.94 to 1.07, which indicates that GO sheets within PANI NF/GO film were successfully reduced.[16, 35, 54]

Having successfully obtained spray-on PANI NF/ERGO electrodes, we next turn to the investigation of their electrochemical properties. Cyclic voltammetry was performed using a three-electrode cell to compare the redox behaviour of a 40-layer pair electrode (970 nm) against a 100-layer pair electrode (3350 nm). The electrolyte was 0.5 M $LiClO_4$ in propylene carbonate, and the counter and reference electrodes were separate lithium metal ribbons. The voltage range was 1.5-4.2 V *vs*. Li/Li$^+$, and the scan rate was 1 mV/s, Figure 4a-b. Both electrodes displayed two distinct symmetric pairs of anodic and cathodic peaks near 3 V and 3.8 V. The peaks are consistent with Faradaic redox reactions attributed to PANI NFs, and are assigned to leucoemeraldine/emeraldine and emeraldine/pernigraniline redox reactions, respectively.[5, 16] The symmetry of both pairs of peaks is indicative of the reversibility

of the redox reaction and the lack of diffusion limitations for under the 1 mV/s scan rate.[4]

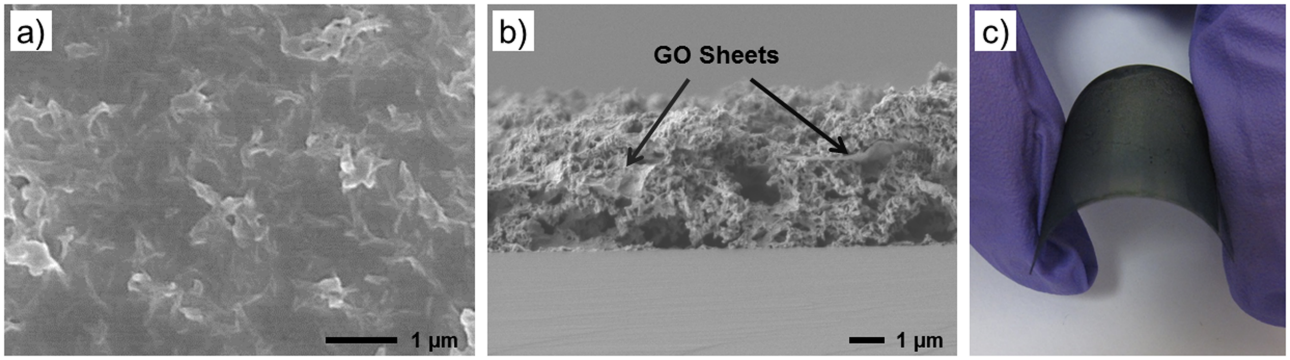

Figure 2. (a) Top-view and (b) cross-sectional–SEM images of PANI NF/GO spray-assisted LbL films, and (c) digital image of a PANI NF/GO spray-assisted LbL film coated onto a flexible PET substrate.

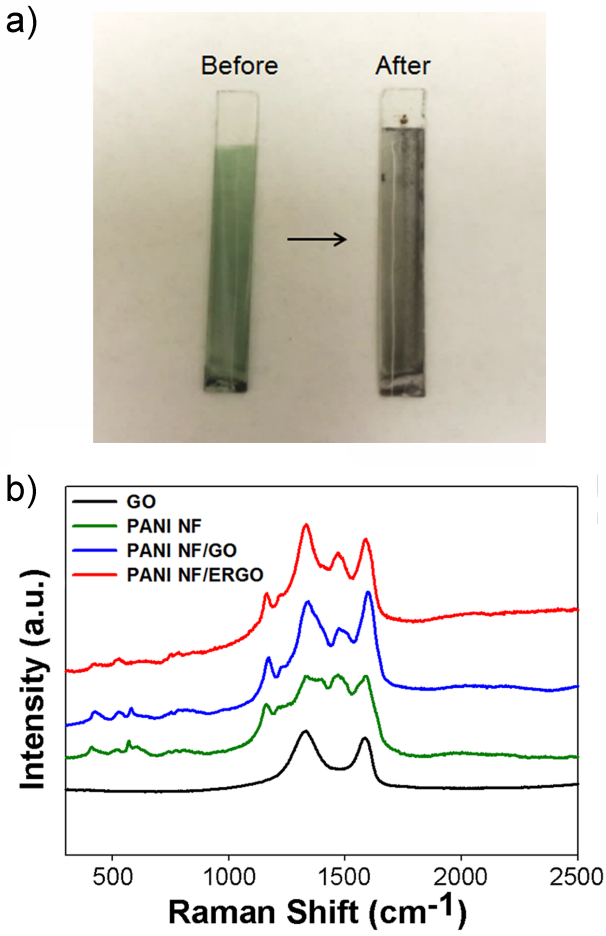

Figure 3. (a) Digital image of a PANI NF/GO spray-assisted LbL film before and after electrochemical reduction. (b) Raman spectra of PANI NFs, GO sheets, PANI NF/GO, and PANI NF/ERGO spray-assisted LbL films.

The two sets of electrodes were then subjected to cyclic voltammetry at scan rates varying from 10 to 100 mV/s. The 40-layer pair electrode exhibited little distortion in its cyclic voltammograms as the scan rate increased, Figure 4c; the cathodic peak at 3.0 V shifted down slightly to 2.8 V at 100 mV/s. On the other hand, the 100-layer pair electrode exhibited severe distortion in its voltammograms, and the cathodic peak shifted substantially from 2.9 V to 2.3 V as scan rate increased, Figure 4d. A plot of the peak current vs. scan rate yielded a linear relationship for both 40 and 100 layer pair electrodes, Figure 4e-f.

The results from cyclic voltammetry demonstrate that thinner electrodes are less susceptible to ion transport limitations as compared to thicker spray-assisted LbL electrodes. The increased distortion and shifted peaks associated with the thicker electrode are consistent with hindered diffusion of ions. On the other hand, the linear relationship of current with scan rate suggests that the redox reaction remains largely pseudocapacitive and surface-confined in nature.[16, 55, 56] As compared to control electrodes made from dip-assisted LbL assembly,[16] the extent of the transport limitation is much less for the sprayed electrodes, likely because they are more porous.

To further understand the nature of charge storage in PANI NF/ERGO spray-assisted LbL electrodes, we performed an analysis of the cyclic voltammograms from Figure 4 such that processes related to diffusion-control and non-diffusion control could be quantitatively separated using a quantity *b*, Figure S2-3. This process is well described in our previous reports and in the ESI.[5, 16] The quantity *b* is equal to unity for non-diffusion control and equal to 0.5 for diffusion control. Both sets of LbL electrodes exhibited *b*-values of 0.8-1.0, and no distinct differences between thick and thin electrodes were observed. This value is supportive of a pseudocapacitive charge storage mechanism with slight diffusion control. On the other hand, *b*-values in comparable electrodes made via dip-assisted LbL assembly were strongly dependent on thickness, for which strong diffusion limitations arose in films even just 1520 nm thick.[16]

Galvanostatic charge-discharge testing was carried out to evaluate the electrochemical performance of the 100-layer pair electrode. Capacity, energy, and power are reported per gram of electrode (PANI NF + ERGO) or per cubic centimetre of electrode (apparent volume). Upon cycling between 1.5 and 4.2 V vs. Li/Li^+, a sloping discharge profile was observed (Figure

5a). This profile is consistent with a pseudocapacitive charge storage mechanism, and is commonly observed for conjugated polymers.[4, 6]

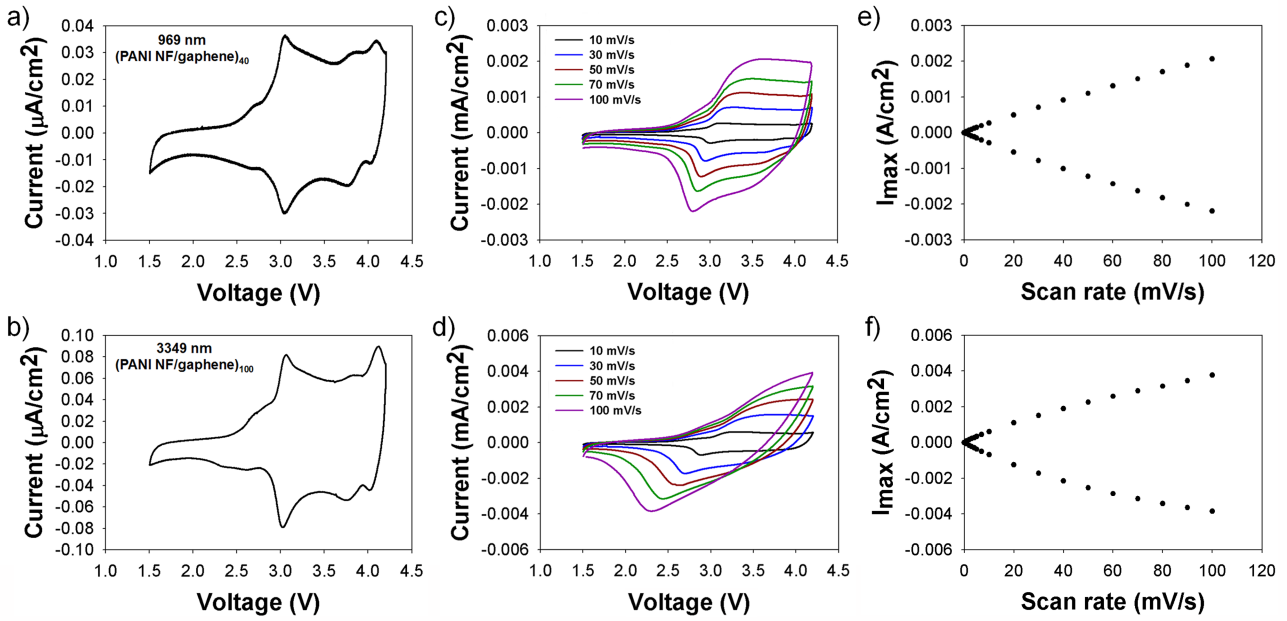

Figure 4. Cyclic voltammograms of PANI NF/ERGO spray-assisted LbL electrodes (a,b) at a scan rate of 1 mV/s and (c,d) at varying scan rates. (e,f) Plots of the maximum current versus scan rate. Panels (a,c,e) correspond to 40-layer pair electrodes (969 nm thick) and panels (b,d,f) correspond to 100-layer pair electrodes (3349 nm thick).

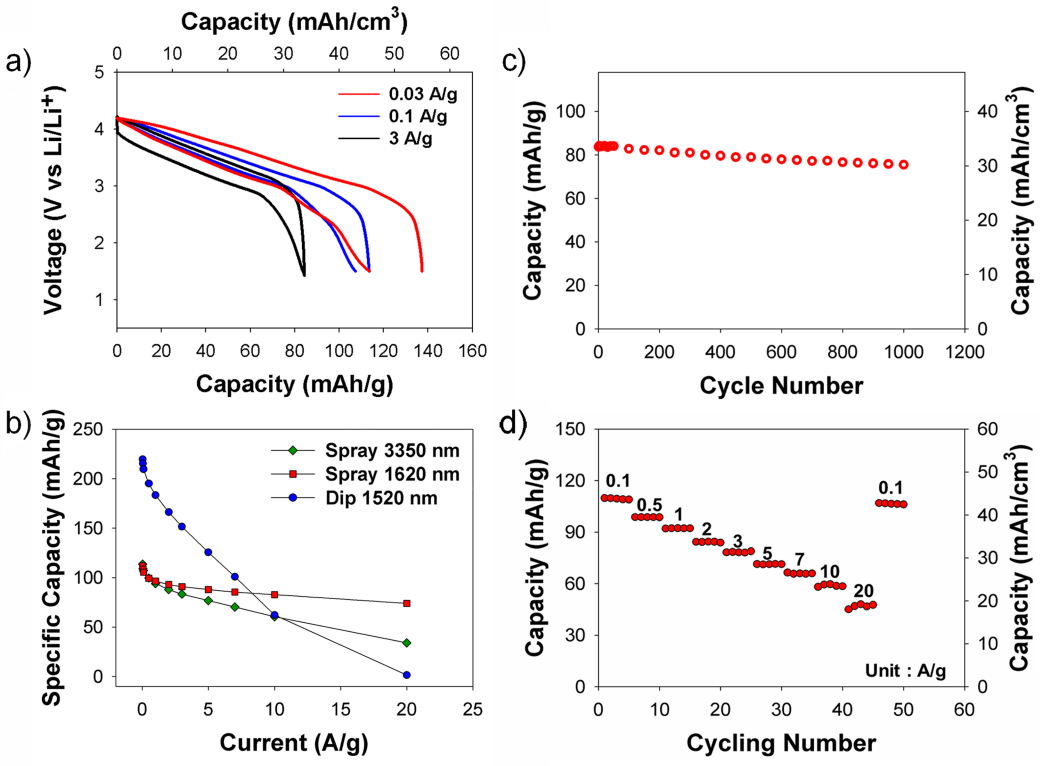

Figure 5. (a) Voltage vs. specific capacity for a 100-layer pair PANI/ERGO spray-assisted LbL electrode at various discharge currents. (b) Specific capacity of a PANI-NF/ERGO dip-assisted LbL electrode compared to various PANI-NF/ERGO spray-assisted LbL electrodes versus discharge current. (c) Cycling behaviour of a 100-layer pair PANI/ERGO spray-assisted LbL electrode at 2 A/g. (d) Galvanostatic cycling of a 100-layer pair PANI/ERGO spray-assisted LbL electrode at varying discharge currents. Data from panels a-c were obtained using a three-electrode cell, and panel d from a two-electrode cell as described in the Experimental Section.

Journal Name

RSCPublishing

ARTICLE

Figure 5b exhibits the specific capacities of 60 and 100-layer pair sprayed electrodes. The 60-layer pair electrode was similar in thickness to a control electrode made by dipping, allowing for a suitable comparison. As the discharge current increased from 0.03 to 20 A/g, the specific capacity of the 100-layer pair sprayed electrode decreased steadily from 114 to 34 mAh/g (45 to 14 mAh/cm^3). The capacity of the 60-layer pair remained fairly steady at 112 to 74 mAh/g. For a similar thickness, the capacity of a control made by dipping precipitously declined from 220 to 1.5 mAh/g as discharge current increased.[16] The spray-assisted LbL electrode clearly demonstrates a better rate capability as compared to dip-assisted LbL electrode, which we attribute to increased porosity brought about by the spray-assembly process.

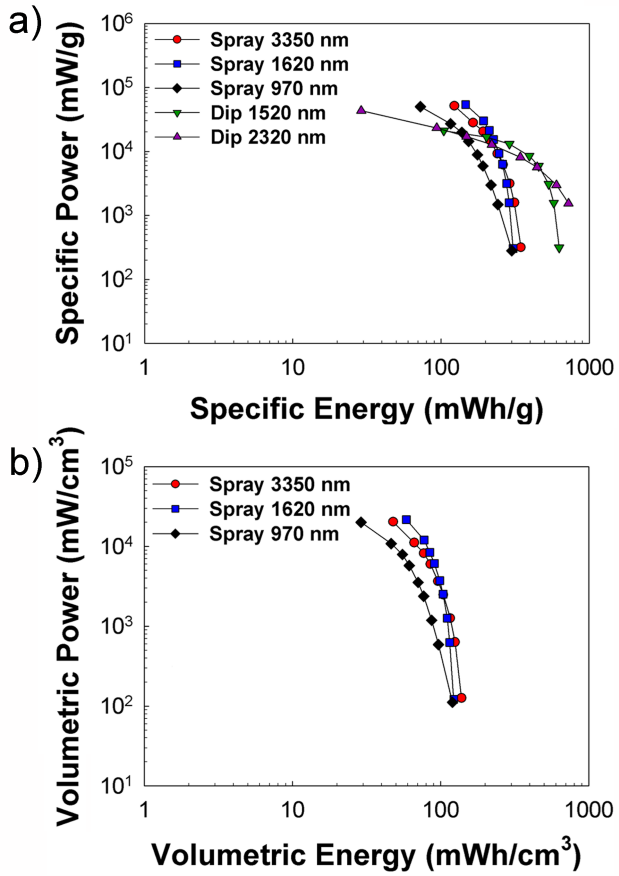

Figure 6. Ragone plots for various PANI NF/ERGO spray-assisted LbL electrodes based on (a) mass and (b) volume. Electrodes were evaluated in two-electrode cells from 1.5-4.2 V, where the anode was lithium metal and the electrolyte was $LiClO_4$ in propylene carbonate. Data from the 1520 nm thick dip-assisted LbL electrode in panel (a) is reproduced from ref. 16.

Accelerated cycling of the 100-layer pair spray-assisted LbL electrode showed an excellent capacity retention of 90% over 1000 cycles, Figure 5c.

To investigate the LbL electrode's behaviour in a practical battery, a lithium metal battery was constructed from a lithium metal anode, a polymer separator, liquid electrolyte and a 100-layer pair PANI NF/ERGO sprayed cathode in a sandwich cell configuration. The sandwich cell was cycled between 1.5 and 4.2 V for various discharge currents (Figure 5d), similar to the conditions experienced in the three-electrode cell. At a current density of 0.1 A/g, the capacity was 110 mAh/g (44 mAh/cm^3). Upon increasing the discharge current to 20 A/g, the capacity decreased by 44%, but the capacity was restored upon returning to 0.1 A/g. The capacity of the electrode in the sandwich cell was generally similar to that in the three-electrode cell at low discharge current.

The energy and power of the spray-assisted LbL electrodes were measured and summarized in Ragone plots based upon electrode mass and apparent electrode volume (Figure 6a-b). The highest specific energy was 346 mWh/g (138 mWh/cm^3) obtained at a discharge current of 0.1 A/g, and the highest specific power was 54090 mW/g (21640 mWh/cm^3) obtained at a discharge current of 20 A/g for the spray-assisted LbL electrode. Compared to dipped LbL electrodes of similar thickness, the sprayed electrode exhibited higher specific power at a given specific energy, confirming the enhanced rate capability of the sprayed LbL electrodes.

CONCLUSION

PANI NF/ERGO electrodes were successfully fabricated *via* spray-assisted LbL assembly of PANI NFs and GO sheets, followed by an electrochemical reduction step. Removal of the rinsing step and addition of a blow-drying step was critical toward the successful deposition of the two nanomaterials by spray. The PANI NF/GO spray-assisted LbL film exhibited linear film growth behaviour (46 nm per layer pair), and the growth rate was 74 times faster than the analogous dipping process. This layer pair thickness was consistent with polyaniline nanofibers adsorbing in a single layer and laying flat against the substrate's surface. The spray-assisted LbL electrodes were less dense and more porous than those made from dipping. Compared with dip-assisted LbL electrodes, spray-assisted LbL electrodes exhibited an improved rate capability and a higher power at a given specific energy, which we attribute to enhanced porosity. The capacity, energy, and power reached values as high as 114 mAh/g (45 mAh/cm^3) at 0.03 A/g, 346 mWh/g (138 mWh/cm^3) at 0.1 A/g, and 54090 mW/g (21640 mW/cm^3) at 20 A/g, respectively.

The spray-assisted LbL process has proven itself to be a rapid fabrication method for the deposition of uniform electrodes onto a variety of substrates, even flexible PET. These sprayed or paintable electrodes, as demonstrated here, raise the prospect of LbL assembly as a versatile tool towards the formation of batteries onto objects of complex shapes for structural energy and power.

Acknowledgements

This work was supported in part by the Air Force Office of Scientific Research (Grant No. FA9550-13-1-0147), the Welch Foundation (A-1766), and 3M Non-Tenured Faculty Award.

Notes and references

*Artie McFerrin Department of Chemical Engineering, Texas A&M University, 3122 TAMU, College Station, TX 77843-3122, United States
*E-mail: jodie.lutkenhaus@che.tamu.edu
† Se Ra Kwon and Ju-Won Jeon contributed equally to this work.
Electronic Supplementary Information (ESI) available: [Analysis of charge storage behaviour related to diffusion/non-diffusion controlled process from cyclic voltammetry, Inner and outer surface charge storage, and movie showing spraying process.]. See DOI: 10.1039/b000000x/

1. N. Singh, C. Galande, A. Miranda, A. Mathkar, W. Gao, A. L. M. Reddy, A. Vlad and P. M. Ajayan, *Sci. Rep.*, 2012, 2.
2. L. Cao, S. Yang, W. Gao, Z. Liu, Y. Gong, L. Ma, G. Shi, S. Lei, Y. Zhang, S. Zhang, R. Vajtai and P. M. Ajayan, *Small*, 2013, 9, 2905-2910.
3. S. Y. Kim, J. Hong, R. Kavian, S. W. Lee, M. N. Hyder, Y. Shao-Horn and P. T. Hammond, *Energy & Environmental Science*, 2013, 6, 888-897.
4. L. Shao, J.-W. Jeon and J. L. Lutkenhaus, *Journal of Materials Chemistry A*, 2014, 2, 14421-14428.
5. J.-W. Jeon, Y. Ma, J. F. Mike, L. Shao, P. B. Balbuena and J. L. Lutkenhaus, *Physical Chemistry Chemical Physics*, 2013, 15, 9654-9662.
6. P. Novák, K. Müller, K. S. V. Santhanam and O. Haas, *Chemical Reviews*, 1997, 97, 207-282.
7. Q. Wu, Y. Xu, Z. Yao, A. Liu and G. Shi, *ACS Nano*, 2010, 4, 1963-1970.
8. D. Li, J. Huang and R. B. Kaner, *Accounts of Chemical Research*, 2008, 42, 135-145.
9. H. D. Tran, D. Li and R. B. Kaner, *Advanced Materials*, 2009, 21, 1487-1499.
10. M. Wan, *Advanced Materials*, 2008, 20, 2926-2932.
11. S. Chaudhari, Y. Sharma, P. S. Archana, R. Jose, S. Ramakrishna, S. Mhaisalkar and M. Srinivasan, *Journal of Applied Polymer Science*, 2013, 129, 1660-1668.
12. Q. Lu, Q. Zhao, H. Zhang, J. Li, X. Wang and F. Wang, *ACS Macro Letters*, 2013, 2, 92-95.
13. H. Mi, X. Zhang, S. Yang, X. Ye and J. Luo, *Materials Chemistry and Physics*, 2008, 112, 127-131.
14. M. N. Hyder, S. W. Lee, F. Ç. Cebeci, D. J. Schmidt, Y. Shao-Horn and P. T. Hammond, *ACS Nano*, 2011, 5, 8552-8561.
15. K. Zhang, L. L. Zhang, X. S. Zhao and J. Wu, *Chemistry of Materials*, 2010, 22, 1392-1401.
16. J.-W. Jeon, S. R. Kwon and J. L. Lutkenhaus, *Journal of Materials Chemistry A*, 2015, DOI: 10.1039/C4TA04697H.
17. J. X. Huang and R. B. Kaner, *Angewandte Chemie-International Edition*, 2004, 43, 5817-5821.
18. A. A. Balandin, S. Ghosh, W. Bao, I. Calizo, D. Teweldebrhan, F. Miao and C. N. Lau, *Nano Letters*, 2008, 8, 902-907.
19. X. Du, I. Skachko, A. Barker and E. Y. Andrei, *Nat Nano*, 2008, 3, 491-495.
20. M. D. Stoller, S. Park, Y. Zhu, J. An and R. S. Ruoff, *Nano Letters*, 2008, 8, 3498-3502.
21. D. A. C. Brownson, D. K. Kampouris and C. E. Banks, *Journal of Power Sources*, 2011, 196, 4873-4885.
22. G. Chen, Z. Zhang, W. Zhai and h. wang, *Journal of Materials Chemistry C*, 2015, DOI: 10.1039/C4TC02471K.
23. S. Stankovich, D. A. Dikin, G. H. B. Dommett, K. M. Kohlhaas, E. J. Zimney, E. A. Stach, R. D. Piner, S. T. Nguyen and R. S. Ruoff, *Nature*, 2006, 442, 282-286.
24. A. S. Arico, P. Bruce, B. Scrosati, J.-M. Tarascon and W. van Schalkwijk, *Nat Mater*, 2005, 4, 366-377.
25. S. W. Lee, B. M. Gallant, H. R. Byon, P. T. Hammond and Y. Shao-Horn, *Energy & Environmental Science*, 2011, 4, 1972-1985.
26. D. Li, M. B. Muller, S. Gilje, R. B. Kaner and G. G. Wallace, *Nat Nano*, 2008, 3, 101-105.
27. K. Sheng, H. Bai, Y. Sun, C. Li and G. Shi, *Polymer*, 2011, 52, 5567-5572.
28. H.-L. Guo, X.-F. Wang, Q.-Y. Qian, F.-B. Wang and X.-H. Xia, *ACS Nano*, 2009, 3, 2653-2659.
29. H. R. Byon, B. M. Gallant, S. W. Lee and Y. Shao-Horn, *Advanced Functional Materials*, 2013, 23, 1037-1045.
30. S. W. Lee, B. M. Gallant, Y. Lee, N. Yoshida, D. Y. Kim, Y. Yamada, S. Noda, A. Yamada and Y. Shao-Horn, *Energy & Environmental Science*, 2012, 5, 5437-5444.
31. S. W. Lee, N. Yabuuchi, B. M. Gallant, S. Chen, B.-S. Kim, P. T. Hammond and Y. Shao-Horn, *Nat Nano*, 2010, 5, 531-537.
32. L. Al-Mashat, K. Shin, K. Kalantar-zadeh, J. D. Plessis, S. H. Han, R. W. Kojima, R. B. Kaner, D. Li, X. Gou, S. J. Ippolito and W. Wlodarski, *The Journal of Physical Chemistry C*, 2010, 114, 16168-16173.
33. J. Cong, Y. Chen, J. Luo and X. Liu, *Journal of Solid State Chemistry*, 2014, 218, 171-177.
34. S. Liu, X. Liu, Z. Li, S. Yang and J. Wang, *New Journal of Chemistry*, 2011, 35, 369-374.
35. X. Yan, J. Chen, J. Yang, Q. Xue and P. Miele, *ACS Applied Materials & Interfaces*, 2010, 2, 2521-2529.
36. G. Decher, *Science*, 1997, 277, 1232-1237.
37. A. K. Sarker and J.-D. Hong, *Langmuir*, 2012, 28, 12637-12646.
38. H. R. Byon, S. W. Lee, S. Chen, P. T. Hammond and Y. Shao-Horn, *Carbon*, 2011, 49, 457-467.
39. S. W. Lee, J. Kim, S. Chen, P. T. Hammond and Y. Shao-Horn, *ACS Nano*, 2010, 4, 3889-3896.

40. S. W. Lee, B.-S. Kim, S. Chen, Y. Shao-Horn and P. T. Hammond, *Journal of the American Chemical Society*, 2008, 131, 671-679.
41. K. C. Krogman, N. S. Zacharia, S. Schroeder and P. T. Hammond, *Langmuir*, 2007, 23, 3137-3141.
42. J. B. Schlenoff, S. T. Dubas and T. Farhat, *Langmuir*, 2000, 16, 9968-9969.
43. W. D. Mulhearn, D. D. Kim, Y. Gu and D. Lee, *Soft Matter*, 2012, 8, 10419-10427.
44. B.-S. Kim, R. C. Smith, Z. Poon and P. T. Hammond, *Langmuir*, 2009, 25, 14086-14092.
45. K. C. Krogman, K. F. Lyon and P. T. Hammond, *The Journal of Physical Chemistry B*, 2008, 112, 14453-14460.
46. T. Otto, P. Mundra, M. Schelter, E. Frolova, D. Dorfs, N. Gaponik and A. Eychmüller, *ChemPhysChem*, 2012, 13, 2128-2132.
47. T. T. Tung, M. Castro, T. Y. Kim, K. S. Suh and J.-F. Feller, *Journal of Materials Chemistry*, 2012, 22, 21754-21766.
48. J. Hong and S. W. Kang, *Journal of Nanoscience and Nanotechnology*, 2011, 11, 7771-7776.
49. T. T. Tung, M. Castro, I. Pillin, T. Y. Kim, K. S. Suh and J. F. Feller, *Carbon*, 2014, 74, 104-112.
50. W. S. Hummers and R. E. Offeman, *Journal of the American Chemical Society*, 1958, 80, 1339-1339.
51. A. Izquierdo, S. S. Ono, J. C. Voegel, P. Schaaf and G. Decher, *Langmuir*, 2005, 21, 7558-7567.
52. S. Pei and H.-M. Cheng, *Carbon*, 2012, 50, 3210-3228.
53. H. Wang, Q. Hao, X. Yang, L. Lu and X. Wang, *Nanoscale*, 2010, 2, 2164-2170.
54. M. Sathiya, A. S. Prakash, K. Ramesha, J. M. Tarascon and A. K. Shukla, *Journal of the American Chemical Society*, 2011, 133, 16291-16299.
55. C. A. Cutler, M. Bouguettaya and J. R. Reynolds, *Advanced Materials*, 2002, 14, 684-688.
56. J.-W. Jeon, J. O'Neal, L. Shao and J. L. Lutkenhaus, *ACS Applied Materials & Interfaces*, 2013, 5, 10127-10136.